MRS Advances (2023) 8:255–260
https://doi.org/10.1557/s43580-023-00544-y

ORIGINAL PAPER

Accelerated dissolution of doped UO_2-based model systems as analogues for modern spent nuclear fuel under repository conditions

Philip Kegler[1] · Stefan Neumeier[1] · Martina Klinkenberg[1] · Andrey Bukaemskiy[1] · Guido Deissmann[1] · Felix Brandt[1] · Dirk Bosbach[1]

Received: 9 January 2023 / Accepted: 9 March 2023 / Published online: 21 March 2023
© The Author(s) 2023

Abstract
Systematic single-effect dissolution studies were carried out on the dissolution behaviour of pure and Cr- or Nd-doped UO_2 reference pellets as model materials for spent nuclear fuel with varying doping levels, densities, and grain sizes as well as of industrially produced Cr- and Cr/Nd-doped UO_2 pellets. The results were obtained from accelerated static batch dissolution experiments performed under strictly controlled conditions using H_2O_2 as simulant for radiolytic oxidants formed due to the alpha-irradiation of water. The results indicate that the addition of Cr and the consequential modification of the fuel matrix does not lead to a significant change of the dissolution behaviour of these model materials compared to pure UO_2 reference materials. Contrarily, the dissolution rates of Nd-doped pellets are significantly lower than those of pure and Cr-doped pellets. These results provide additional insights into the influence of doping on the dissolution behaviour of modern spent light water reactor fuels under the post-closure conditions expected in a deep geological repository.

Introduction

Due to the extremely high level of radioactivity of spent nuclear fuel (SNF), dominated by β- and γ-radiation, systematic experimental studies on mechanisms governing the long-term matrix corrosion of SNF are challenging [1]. The needs for extensive radiation shielding and remote handling, and the often limited amounts of SNF available for experimental studies allow generally only for a limited number of dissolution experiments. This hampers micro-analytical and micro-structural investigations of the materials prior and after dissolution experiments. Moreover, high-burn-up fuels or irradiated modern light water reactor (LWR) fuels doped, e.g., with Cr_2O_3 or Al_2O_3, are even less available so far for such experiments [2]. While the improved in-reactor performance of these fuels has already been demonstrated [3–5], their corrosion/dissolution behaviour in a deep geological repository (DGR) in comparison to conventional spent LWR-fuels is not completely understood. However, experiments with SNF cannot unravel all concurring processes effecting the dissolution mechanism in aqueous media, due to the chemical and structural complexity of SNF. In addition, "fresh" SNF is associated with a high α, β- and γ-radiation field. At the earliest time at which a failure of the waste container in a DGR is to be expected, SNF in a nominally reducing repository environment will come into contact with water and the radiation field will be dominated by α-radiation leading to water radiolysis [6–11]. Thus, complementary to experiments on doped SNF, dedicated dissolution studies are required using systematically produced and carefully characterised UO_2-based model materials to understand the effects of the addition of Cr- or Ln^{3+}-oxides into the fuel matrix on the SNF dissolution behaviour under conditions expected in a DGR post-closure. In this study, these model materials comprised (i) UO_2 reference materials, and (ii) Cr- and Nd-doped UO_2. Single-effect studies on the dissolution behaviour of the model materials provided complementary insights and supporting process understanding regarding the performance of modern doped fuels in the repository environment, which cannot be directly obtained from dissolution studies on SNF.

✉ Philip Kegler
p.kegler@fz-juelich.de

[1] Forschungszentrum Jülich GmbH, Institute of Energy and Climate Research—Nuclear Waste Management (IEK-6), 52428 Jülich, Germany

Materials and methods

Within this work no experiments on human and animal subjects are reported.

For all experiments chemicals with very high purity grade (99.9% or higher) were used and obtained from Merck, Emsure®, Sigma Aldrich and Honeywell Fluka. Previously degassed Millipore Milli-Q filtered water (18.2 MΩ resistivity, Elga PURELAB Ultra installation) was used throughout. The synthesis of the UO_2 model materials with and without Cr- and Nd-doping for the dissolution experiments is described in detail in Kegler et al. [12] and is summarised only briefly here. The pure and the doped materials were synthesised using a (co-)precipitation method (CPM), where the metal ions in the desired mixture are quantitatively precipitated as pure or doped ammonium-diuranate (ADU). After several washing steps the dried ADU powder was calcined at 600 °C or 800 °C for 5 h in air to form U_3O_8. Subsequently U_3O_8 was reduced to UO_2 in a second calcination step at 600 °C for another 5 h in reducing atmosphere (4% H_2 in Ar). For samples doped with wet coating method (WCM) the dopant was added after this step and the previous steps of thermal treatment were repeated. Finally, the calcined powder was compacted to pellets and sintered at 1700 °C for 10 h in reducing atmosphere. No information is available about the preparation method of the commercially available Cr- and Cr/Nd-doped pellets (AREVA) used as reference industrial samples for the dissolution experiments in this work. A compilation of the samples and their properties is given in Table 1. The pellets used for the dissolution experiments have a diameter of approximately 8.5 mm and a thickness of approximately 1.5 mm, except the commercially available pellets purchased from AREVA (approx. 9.2 mm diameter, approx. 1.8 mm height). One site of the pellet was polished mirror like, whereas the other side was only grinded by a P1200 sandpaper (ISO designation, average grainsize 15.3 µm).

Table 1 UO_2 pellets used for dissolution experiments and their properties

Sample	Doping Cr_2O_3/Nd_2O_3 (wt. ppm)	Doping method	Oxygen pot (kJ mol^{-1} O_2)	T.D. (%)	Grain size (µm)	Height (mm)	Diameter (mm)	Geom. surf. (mm^2)	Initial dissolution rate (mol s^{-1} m^{-2})
SL-DC-19-2	Pure UO_2	–	− 510	93.50	12	1.38	8.36	146.03	1.79×10^{-06}
SL-DC-19-3	Pure UO_2	–	− 510	94.00	12	1.51	8.52	154.44	1.69×10^{-06}
SL-DC-19-4	Pure UO_2	–	− 510	94.60	12	1.48	8.49	152.70	1.62×10^{-06}
SL-DC-19-5	Pure UO_2	–	− 510	95.00	12	1.54	8.64	159.06	1.40×10^{-06}
SL-DC-35-1	Pure UO_2	–	− 420	96.48	12	1.24	8.46	145.38	1.16×10^{-06}
SL-DC 18-1	1000	CPM	− 510	95.85	12	1.55	8.30	148.50	1.06×10^{-06}
SL-DC-18-5	1000	CPM	− 510	97.61	12	1.36	8.48	149.19	7.78×10^{-07}
SL-DC-22-7	1000	WCM	− 510	98.75	19	1.38	8.45	148.79	6.98×10^{-07}
SL-DC-33-1	1000	CPM	− 420	97.01	20	1.19	8.53	146.18	6.49×10^{-07}
SL-DC 33-2	1000	CPM	− 420	97.02	20	1.26	8.50	147.14	1.23×10^{-06}
SL-DC 36-1	1000	WCM	− 420	97.02	24	1.32	8.45	147.20	1.54×10^{-06}
SL-DC 47-2	1500	WCM	− 420	98.50	38	1.58	8.30	149.41	1.66×10^{-06}
SL-DC 47-6	1500	WCM	− 420	98.50	38	1.60	8.33	150.87	1.39×10^{-06}
SL-DC 47-7	1500	WCM	− 420	98.50	38	1.50	8.32	147.94	1.58×10^{-06}
SL-DC 47-9	1500	WCM	− 420	98.50	38	1.40	8.32	145.33	1.83×10^{-06}
SL-DC 37-2	2500	WCM	− 420	98.35	69	1.16	8.38	140.85	5.55×10^{-07}
SL-DC 23-2	5000 Nd_2O_3	CPM	− 510	98.19	ND	1.61	8.33	151.13	2.17×10^{-07}
SL-DC 24-1	10,000 Nd_2O_3	CPM	− 510	98.55	ND	1.58	8.33	150.34	1.11×10^{-07}
SL-DC 24-2	10,000 Nd_2O_3	CPM	− 510	98.55	ND	1.28	8.30	141.59	1.30×10^{-07}
AREVA 1	1500	?	?	96.20	37	1.74	9.20	183.24	1.48×10^{-06}
AREVA 2	950 Cr + 1300 Nd	?	?	94.20	10	1.86	9.26	188.80	1.6478E−07

The last column shows the initial dissolution rate determined for the first 24 h of the experiments. Doping Cr_2O_3 and/or Nd_2O_3 = amount of initial Cr_2O_2/Nd_2O_3 doping given in wt. ppm

Doping method: CPM—co-precipitation method, WCM—wet coating method, Oxygen pot.—oxygen potential during sinter process, T.D.—theoretical density, geom. surf.—geometrical surface area, ?—unknown

Accelerated dissolution experiments [7–11, 13] with UO_2 model materials with and without Cr-doping synthesised in the framework of this work were carried out as static batch experiments in previously degassed bicarbonate solutions ($NaHCO_3$, 10 mmol L^{-1}), using hydrogen peroxide (H_2O_2, 2.25 mmol L^{-1}) to mimic the oxidative radiolytic dissolution of UO_2. A detailed description of the experimental procedure can be found in [13].

The experimental setup optimized for these dissolution experiments is shown in Fig. 1 and aimed in particular at (1) maintaining the pellets completely covered with test solution throughout the whole dissolution experiments, (2) allowing easy sampling of test solution and permanent flushing of the vessels with argon, (3) providing light tight vessels to ensure constant conditions regarding H_2O_2 degradation during the experiments, and (4) controlling the experimental temperature. During the experiment the temperature was kept constant at 22 °C.

The setup allows for the accomplishment of 11 dissolution experiments in parallel. The sample vessels were placed in a massive aluminium block equipped with a water conduit connected to a thermostat for temperature control. Plasticine gaskets were used to close the contact between the vessels and aluminium block and to ensure the light tightness of the vessels. To achieve anoxic conditions the solutions were flushed with argon during the complete experimental run time. In all experimental runs performed to date, 8 vessels were used for dissolution tests (Fig. 1a, blue gaskets) with UO_2 based pellets, while 3 vessels were used as blanks to monitor the bulk degradation of H_2O_2 (Fig. 1a, red gaskets) which is needed for the later calculation of the dissolution yield. During the dissolution experiments, solutions were systematically sampled and the H_2O_2 (UV–Vis, Perkin Elmer, Lambda 19) and the uranium (ICP-MS, Perkin Elmer, NexION 2000) concentrations were determined.

The driving force for the UO_2 dissolution in that kind of accelerated dissolution experiment is the oxidative potential of H_2O_2 which is proportional to its concentration in solution. In the experiments the $NaHCO_3$ in the solution represents the bicarbonate contained in groundwater. It additionally serves the purpose to prevent the precipitation of U(+VI) phases, and therefore, to ensure a reliable measurement of the uranium concentration in solution. Bicarbonate does not intervene directly in the oxidation process, but—with oxidative dissolution—complexes the dissolved U(+VI) and thus influences the kinetics/driving force, so that the dissolution rate increases with the bicarbonate concentration [14]. Therefore, the NaHCO3 concentration was kept constant to 10 mmol L^{-1} in all experiments.

The end of the dissolution process is marked by the accomplishment of a constant uranium concentration in the solution. As stated before, this plateau is not due to the limit of U(+VI) solubility, but due to the complete consumption of H_2O_2 in the solution. Due to the previously discovered surface passivation effect when repeatedly employing the same pellets in the dissolution tests, only results from dissolution experiments using pristine pellets were considered for determining the dissolution rates [13].

Results

The accelerated dissolution experiments in this work were conducted using pure, Cr- and Nd-doped UO_2 pellets, as well as commercially available Cr- and Cr- plus Nd-doped UO_2 pellets.

In Fig. 2 the uranium concentration in solution normalised to the geometrical surface area (a) and the H_2O_2 concentration (b) is plotted as a function of the first 300 h of dissolution experiments using pellets with different compositions. Red circles represent experiments with pure UO_2, diamonds experiments using pellets doped with the wet coating method (representative for all Cr-doped UO_2 pellets). The blue colour indicates that the samples used for the experiments were Cr-doped, green symbols represent Nd-doping. The yellow stars in Fig. 2b represent the H_2O_2 concentration in solution of a blank experiment.

All plots show a typical trend over time. Within the first 100 h, a significant increase of the uranium and decrease of the H_2O_2 concentration is evident (initial dissolution phase),

Fig. 1 **a** Experimental setup of the dissolution experiments. **b** Schematic drawing of the vessels for the accelerated dissolution experiments

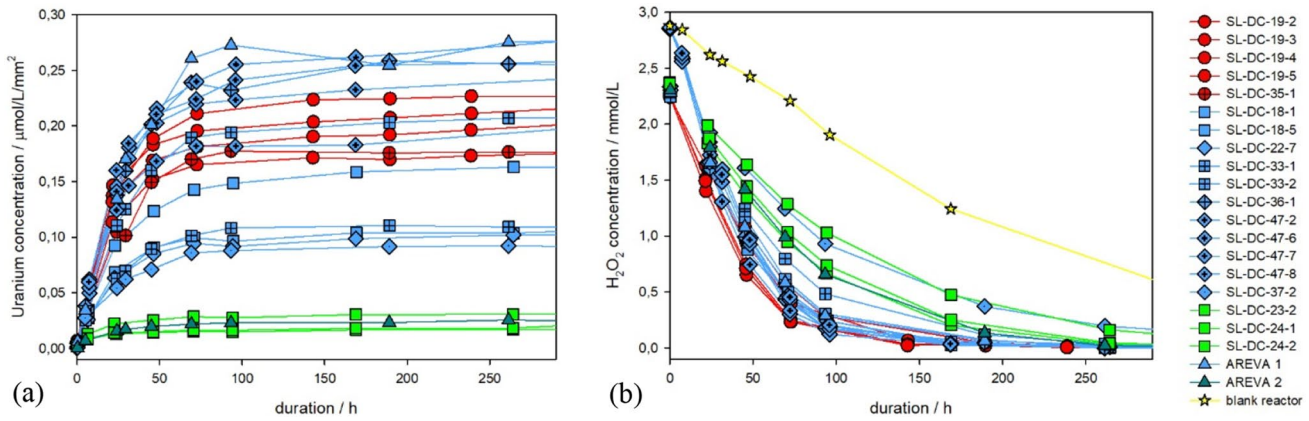

Fig. 2 **a** Uranium concentration in solution normalised to the geometrical pellet surface versus experimental duration. **b** H_2O_2 concentration in solution. The properties of the samples are listed in Table 1. Symbol code: circles—pure UO_2 samples, squares—samples doped via co-precipitation method, diamonds—samples doped via wet coating method, triangles—commercially available samples, star—blank reactor (only H_2O_2). Colour code: red—pure UO_2, blue—Cr-doped, green—Nd-doped, yellow—blank reactor (only H_2O_2)

while after 100 h the uranium and hydrogen peroxide concentration reach a constant value (steady state phase of the dissolution experiment). The initial dissolution phase is caused by preferred dissolution of highly activated surface sites of the pellets and the consumption of the hydrogen peroxide. Apparently, the dissolution is closely linked to the decrease of H_2O_2 due to the oxidation of U(+IV) to U(+VI) on the pellet's surface. A comparison with the consumption of H_2O_2 in the blank experiment (yellow stars in Fig. 2b) shows a distinctly higher H_2O_2 consumption for experiments with UO_2 pellets. This difference can be explained by the additional surface of the pellet, which is missing in the blank experiment, and by the oxidation from U(+IV) to U(+VI). The almost linearly decreasing H_2O_2 concentration in the blank experiment is caused by the decomposition of H_2O_2 and confirms that H_2O_2 is the driving force of the dissolution mechanism of UO_2 in aqueous media. For most experiments the plateau after 100 h marks the end of these dissolution experiments because most of the hydrogen peroxide is consumed by the oxidation of UO_2 or is decomposed (H_2O_2 concentration < 0.3 mmol L^{-1}). The experiments with Cr-doped UO_2 show no significant difference in the solution behaviour of uranium to the experiments conducted with pure UO_2 pellets. The surface normalised uranium concentration in solution after accomplishment of the plateau is between 0.08 and 0.26 µmol L^{-1} mm^{-2}. The mean initial dissolution rate for the experiments performed on pellets with and without Cr-doping is $1.24 \pm 0.4 \cdot 10^{-6}$ mol s^{-1} m^{-2} (RSD = 32.6%). The mean initial dissolution rate determined for the commercially available pellets are in good accordance with the values determined for pellets produced within this work. The distinct changes in the microstructure caused by Cr-doping (see Table 1) do not seem to have any significant influence on the dissolution behaviour of the UO_2 matrix. Remarkably, in all experiments on Nd-bearing UO_2 pellets significantly lower surface normalised uranium concentrations between 0.029 and 0.015 µmol L^{-1} mm^{-2} were detected after reaching the steady state plateau. The mean initial dissolution rate for these experiments is $1.63 \pm 0.7 \times 10^{-7}$ mol s^{-1} m^{-2} (RSD = 25.9%).

This effect is much better understandable if the dissolution yield is taken into account. The dissolution yield is the measure of the amount of H_2O_2 that oxidises U (+IV) to U (+VI) compared to the amount of H_2O_2 that decays at the sample surface in the same time period without oxidising uranium. It is estimated as the ratio of the amount of U(+VI) dissolved from a pellet and the amount of H_2O_2 consumed on the same solid specimen. To determine this quantity, identical blank experiments without a sample must be performed in parallel with the dissolution experiments to determine the degradation of H_2O_2 at the surfaces in the experimental vessel. This amount of decayed H_2O_2 is subtracted from the determined H_2O_2 degradation in the experiment with sample to only consider the influence of the sample. With this quantity the efficiency of the oxidation process of U(+IV) to U(+VI) using H_2O_2 is expressed [15]. In Fig. 3 the dissolution yield is plotted as a function of the degree of initial doping.

The dissolution yields of the pure and the Cr-doped materials including the commercial pellet is mainly in the range between 0.7 and 3.0%. In contrast, the dissolution yield derived from the experiments with the Nd-doped samples (incl. the commercial pellet) is below 0.5%. This observation is underlined by the relatively high H_2O_2 concentration measured for the Nd-doped samples over the temporal evolution of the dissolution experiments (cf. Figure 2b green squares and green triangle). Apparently, much less H_2O_2 is consumed for the oxidation of UO_2 due to doping

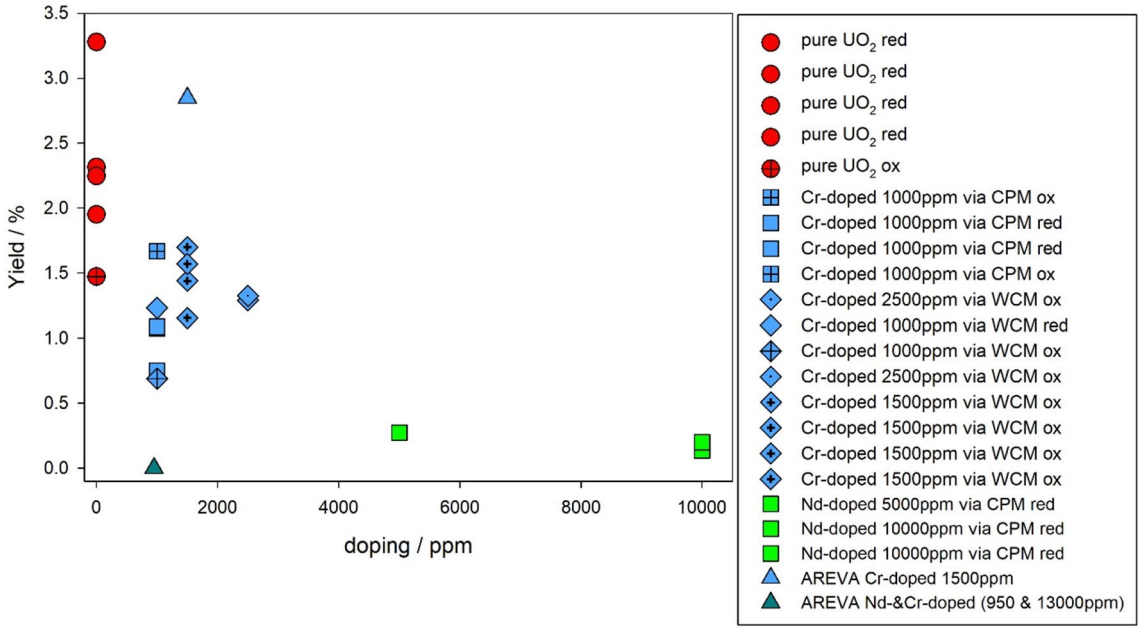

Fig. 3 Dissolution yield as a function of degree of initial doping, Symbol code: circles—pure UO_2 samples, squares—samples doped via co-precipitation method, diamonds—samples doped via wet coating method, triangles—commercially available samples. Colour code: red—pure UO_2, blue—Cr_2-doped, green—Nd-doped

with trivalent Nd^{3+} ions. It seems that the doping of Nd^{3+} is stabilising the UO_2 structure and prevent U(+IV) from oxidation [16].

Conclusion

The dissolution kinetics of pure, Cr- as well as Nd-doped UO_2 pellets prepared by co-precipitation and wet-coating methods were investigated at room temperature in bicarbonate solutions using hydrogen peroxide to mimic the oxidative radiolytic dissolution of UO_2. The investigations on these model systems show no evidence that the Cr-doping leads to a change in the dissolution behaviour i.e., normalised dissolution rates and yields of pure UO_2 and Cr-doped UO_2 pellets are in the same order of magnitude. In contrast, the Nd-doped UO_2 pellets have a distinctly lower initial dissolution rates and yields which implies that less UO_2 is oxidised in these samples. Apparently, Nd^{3+} is stabilising the UO_2 structure. From these results it can be concluded that also doping of UO_2 with Gd^{3+}, which is used as burnable neutron poison in advanced nuclear fuels due to its very high neutron cross section, would probably lead to a comparable stabilisation of the UO_2 like Nd^{3+}, because of the very similar ionic radii and the chemical behaviour of both lanthanides [17, 18].

Acknowledgments This project has received funding from the European Union's Horizon 2020 research and training programme of the European Atomic Energy Community (EURATOM) (H2020-NFRP2016/2017) under grant agreement No. 755443 (DisCo). Open Access funding was enabled and organized by Projekt DEAL.

Funding Open Access funding enabled and organized by Projekt DEAL.

Data availability The raw datasets generated during and/or analysed during the current study are available from the corresponding author on reasonable request.

Declarations

Conflict of interest On behalf of all authors, the corresponding author states that there is no conflict of interest.

Open Access This article is licensed under a Creative Commons Attribution 4.0 International License, which permits use, sharing, adaptation, distribution and reproduction in any medium or format, as long as you give appropriate credit to the original author(s) and the source, provide a link to the Creative Commons licence, and indicate if changes were made. The images or other third party material in this article are included in the article's Creative Commons licence, unless indicated otherwise in a credit line to the material. If material is not included in the article's Creative Commons licence and your intended use is not permitted by statutory regulation or exceeds the permitted use, you will need to obtain permission directly from the copyright holder. To view a copy of this licence, visit http://creativecommons.org/licenses/by/4.0/.

References

1. D. Shoesmith: in Uranium: Cradle to Grave, edited by P.C. Burns, G. E. Sigmon (Mineralogical Association of Canada), vol. 43p. 337p (2013)
2. K. Nilsson, O. Roth, M. Jonsson, J. Nucl. Mater. **488**, 123–128 (2017)
3. Commissariat à l'énergie atomique (CEA), Nuclear fuels. A Nuclear Energy Division Monograph. Gif-sur-Yvette, 147 pp. (2009)
4. J. Arborelius, K. Backman, L. Hallstadius, M. Limbäck, J. Nilsson, B. Rebensdorff, G. Zhou, K. Kitano, R. Löfström, G. Rönnberg, J. Nucl. Sci. Tech. **43**, 967–976 (2006)
5. A.R. Massih, Effects of additives on uranium dioxide fuel behavior. SSM Report **21**, 62 (2014)
6. H.U. Zwicky, J. Low, J.E. Ekeroth, Corrosion studies with high burnup light water reactor fuel, SKB TR-11-03, Svensk Kärnbränslehantering AB, (2011)
7. M. Trummer, B. Dahlgren, M. Jonsson, J. Nucl. Mater. **407**, 195–199 (2010)
8. R. Pehrman, M. Amme, O. Roth, E. Ekeroth, M. Jonsson, J. Nucl. Mater. **397**, 128–131 (2010)
9. S. Nilsson, M. Jonsson, J. Nucl. Mater. **410**, 89–93 (2011)
10. C.M. Lousada, M. Trummer, M. Jonsson, J. Nucl. Mater. **434**, 434–439 (2013)
11. Y. Kumagai, A. Barreiro Fidalgo, M. Jonsson, J. Phys. Chem. C **123**, 9919–9925 (2019)
12. P. Kegler, M. Klinkenberg, A. Bukaemskiy, G.L. Murphy, G. Deissmann, F. Brandt, D. Bosbach, Materials **14**, 6160 (2021)
13. A.C. Maier, P. Kegler, M. Klinkenberg, A. Baena, S. Finkeldei, F. Brandt, M. Jonsson, Dalton Trans. **49**, 1241 (2020)
14. E. Ekeroth, M. Jonsson, J. Nucl. Mater. **322**, 242–248 (2003)
15. M. Jonsson, E. Ekeroth, O. Roth, MRS Proc. **807**, 77 (2003)
16. V.L. Vinograd, A.A. Bukaemskiy, G. Modolo, G. Deissmann, D. Bosbach, Front. Chem. **9**, 705024 (2021)
17. A.B. Fidalgo, M. Jonsson, J. Nucl. Mater. **514**, 216–223 (2019)
18. N. Rodríguez-Villagra, O. Riba, A. Milena-Pérez, J. Cobos, L. Jimenez-Bonales, S. Fernández-Carretero, E. Coene, O. Silva, L. Duro, J. Nucl. Mater. **568**, 153880 (2022)

Publisher's Note Springer Nature remains neutral with regard to jurisdictional claims in published maps and institutional affiliations.